Regular Article

Multi-Objective Optimization for IRS-Aided Multi-user MIMO SWIPT Systems

Pham Van Quyet[1,2], **Ha Hoang Kha**[1,2]

[1] Ho Chi Minh City University of Technology (HCMUT), 268 Ly Thuong Kiet Street, District 10, Ho Chi Minh City, Vietnam
[2] Vietnam National University Ho Chi Minh City, Linh Trung Ward, Thu Duc City, Ho Chi Minh City, Vietnam

Correspondence: Ha Hoang Kha, hhkha@hcmut.edu.vn
Communication: received 03 September 2023, revised 08 December 2023, accepted 24 December 2023
Online publication: 26 December 2023, Digital Object Identifier: 10.21553/rev-jec.337
The associate editor coordinating the review of this article and recommending it for publication was Prof. Hoang Van Phuc.

Abstract– **In this paper, we investigate an intelligent reflecting surface (IRS) assisted simultaneous wireless information and power transfer (SWIPT) system in which users equipped with multiple antennas exploit power-splitting (PS) strategies for simultaneously information decoding (ID) and energy harvesting (EH). Different from the majority of previous studies which focused on single objective optimization problems (SOOPs) and assumed the linearity of EH models, in this paper, we aim at studying the multi-objective optimization problem (MOOP) of the sum rate (SR) and the total harvested energy (HE) subject to the maximum transmit power (TP) constraint, the user quality of service (QoS), and HE requirements at each user with taking a practical non-linear EH (NLEH) model into consideration. To investigate insightful tradeoffs between the achievable SR and total HE, we adopt the modified weighted Tchebycheff method to transform the MOOP into a SOOP. However, solving the SOOPs and modified SOOP is mathematically difficult due to the non-convexity of the object functions and the constraints of the coupled variables of the base station (BS) transmit precoding matrices (TPMs), the user PS ratios (PSRs), and the IRS phase shift matrix (PSM). To address these challenges, an alternating optimization (AO) framework is used to decompose the formulated design problem into sub-problems. In addition, we apply the majorization-minimization (MM) approach to transform the sub-problems into convex optimization ones. Finally, numerical simulation results are conducted to verify the tradeoffs between the SR and the total amount of HE. The numerical results also indicate that the considered system using the IRS with optimal phase shifts provides considerable performance improvement in terms of the achievable SR and HE as compared to the counterparts without using the IRS or with the IRS of fixed phase shifts.**

Keywords– **Intelligent reflecting surfaces (IRS), multi-user MIMO, simultaneously wireless information and power transfer (SWIPT), multi-objective optimization problem (MOOP).**

1 Introduction

The significant growth in applications and services within wireless communications has been a key driving force for the development of advanced technologies. Massive multiple-input multiple-output (MIMO) technologies which are recognized as one of the effective solutions to increase spectral efficiency (SE) have been studied and deployed in wireless communication systems (WCSs) [1]. However, the exploitation of the large number of antennas leads energy consumption issues. Apart from the SE, the design of WCSs recently has paid more attention to energy efficiency (EE) issues to move towards next generation of green WCSs. With the rapid development of advanced metasurfaces and fabrication technologies, intelligent reflecting surfaces (IRSs) have arisen as a promising approach to boost the WCS performance [2]. An IRS is composed of a vast number of programable elements which are capable of reflecting incident radio-frequency (RF) waves and changing their phase shifts [3, 4]. Through precise adjustment of the phase shifts, the signals reflected from the IRS can be effectively combined with other signal links, either constructively or destructively, based on specific requirements of WCSs [5, 6]. Consequently, propagation environments can be smartly controlled to establish favourable channels. In addition, IRSs can easily integrate into existing wireless networks due to their flexibility and low implementation cost [5, 7].

Apart from the goals of the SE and EE, WCS designs aim at prolonging the lifetime of wireless devices by harvesting energy from surrounding environment. To this end, recent studies have focused on simultaneous wireless information and power transfer (SWIPT) techniques [8–10]. In general, SWIPT has two basic schemes, namely a separated scheme and a co-located scheme [11, 12]. In the separated scheme, there are two groups of users, namely energy harvesting (EH) users and information decoding (ID) users, in which each receiver has a distinct function of either EH or ID. Conversely, in the co-located scheme, each device conducts both EH and ID functions through either time switching or power splitting (PS) methods.

1.1 Related Works

The studies on deploying IRSs in SWIPT systems for various scenarios have been reported in [5, 13, 14]. In [5], the authors studied an IRS-assisted SWIPT multi-user MIMO system in which the transmit precoding matrices (TPMs) at the base station (BS) and phase shift matrix (PSM) of the IRS are jointly optimized to maximize the weighted sum rate (SR) of the information receivers. To address the challenges caused by the non-convex characteristics of the optimization problem (OP), the authors in [5] employed the block coordinate descent algorithm for decoupling the original OP into multiple sub-problems and alternatively optimized the TPMs and the PSM. The authors in [13] proposed a penalty-based algorithm to minimize the total transmit power (TP) under the quality-of-service (QoS) constraints and the EH constraints for all users. In [14], the max-min EE of the IRS-aided SWIPT system was investigated, where the authors proposed two algorithms, namely penalty-based and inner approximation-based strategies, to handle the non-convexity of the OP. Similarly, the authors in [15] studied the harvested energy (HE) maximization in IRS-assisted SWIPT multi-user MIMO systems. Notice that all of the aforementioned works focus on optimizing a sole system performance metric referred to as a single objective OP (SOOP), while only a few papers considered simultaneous OPs of conflicting objectives, namely a multi-objective OP (MOOP) [16–18].

1.2 Contributions

Motivated by the aforementioned discussion, the present paper delves into an IRS-aided MU-MIMO SWIPT system with the non-linear EH (NLEH) model. The co-located SWIPT scheme is deployed, in which the users adopt the PS method to conduct both ID and EH simultaneously. To investigate the insights on tradeoffs between the achievable SR and sum HE (SHE), we formulate the design problem as a MOOP of the SR maximization (SRM) and sum HE maximization (SHEM). It is important to highlight that MOOP design is a necessary research trend in next generation wireless systems in which various conflicting performance metrics are taken into consideration [19, 20]. To emphasize the distinctiveness of our research, we compare it with the other related works in Table I. The contributions of our work can be described as follows:

- We formulate the design problems of the BS TPMs, user PS ratios (PSRs), and IRS PSM to maximize the SR and sum HE under the constraints of maximum TP, the minimum user rate requirement, the minimum user HE requirement and IRS unit-modulus. Both SOOPs and MOOP are formulated as non-convex non-linear constrained OPs whose optimal solutions cannot be directly obtained.
- To investigate Pareto optimal solutions, we transform the MOOP into the SOOP by using the modified weighted Tchebycheff (MWT) method [21]. The resultant SOOPs and MOOP under consideration are highly complicated to solve since the coupling of the design variables, the non-convexity of the objective functions (OFs) and constraints. To tackle these issues, an alternating optimization (AO) framework is utilized to alternately optimize the BS TPMs, the user PSRs, and the IRS PSM. To deal with the non-convexity property of each sub-problem, we exploit the majorization-minimization (MM) method to determine lower bound concave functions for the NLEH and user rate functions and establish the convex inner counterparts of the feasible sets to recast the OPs as convex forms.
- Simulations are provided to illustrate the benefits of employing optimal IRS for enhancing SR and HE performance. In addition, the simulation results provide the insightful performance tradeoffs between the SR and HE performance in the considered system.

The structure of this paper is outlined as follows. Section 2 describes the signal and system model. In Section 3, the design OPs for SOOPs composed of the SRM and SHEM are formulated. Then, the MOOP of the SRM and SHEM is devised. Section 4 develops the iterative algorithms to solve the considered SOOPs and MOOP. Finally, Section 5 provides the simulation results while Section 6 offers the concluding remarks.

Notations: The trace, determinant, Hermitian transpose, and transpose operations of a matrix $\mathbf{X}$ are expressed as $\mathrm{Tr}(\mathbf{X})$, $|\mathbf{X}|$, $\mathbf{X}^H$, and $\mathbf{X}^T$ respectively. The identity matrix of dimension $n \times n$ is represented by $\mathbf{I}_n$ while a diagonal matrix with the main diagonal entries of a_1, a_2, ..., a_M is written as $\mathrm{diag}(a_1, a_2, \cdots, a_M)$. The Hadamard product of two matrices $\mathbf{X}$ and $\mathbf{Y}$ is represented by $\mathbf{X} \odot \mathbf{Y}$. Expression $\mathbf{X} \succeq \mathbf{0}$ stands for a positive semi-definite matrix $\mathbf{X}$. An expectation operation is expressed by $\mathbb{E}(\cdot)$. $\mathbf{x} \sim \mathcal{CN}(\mathbf{a}, \mathbf{R})$ stands for a complex Gaussian random vector $\mathbf{x}$ with mean $\mathbf{a}$ and covariance matrix $\mathbf{R}$. With function $f(\mathbf{X}, \mathbf{Y})$, it is referred to as $f(\mathbf{X})$ when $\mathbf{Y}$ is fixed.

2 System Model

The considered IRS-aided MU-MIMO SWIPT system is sketched in Figure 1 in which a BS having N_t antennas communicates with L multiple antenna users (UEs) in downlinks with the assistance of an IRS of N reflecting elements. User ℓ denoted by UE_ℓ with

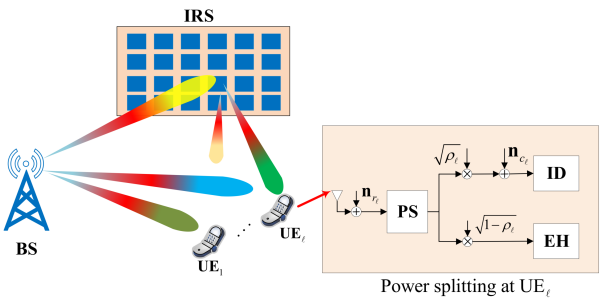

Figure 1. A multi-user MIMO SWIPT system with the assistance of the IRS.

Table I
Comparison of This Work with the Related Works

	[5]	[14]	[15]	[16]	[17]	[18]	This work
MIMO	✓	X	✓	X	X	X	✓
SOOP	✓	✓	✓	✓	✓	✓	✓
MOOP	X	X	X	✓	✓	✓	✓
Co-located SWIPT	X	✓	✓	X	X	X	✓
NLEH model	X	✓	✓	X	X	X	✓
Minimum HE constraints	✓	✓	✓	X	X	✓	✓
Minimum data rate constraints	X	✓	✓	X	X	✓	✓

$\ell \in \mathcal{L} = \{1, \cdots, L\}$ is equipped with N_r antennas. By applying the TPM $\mathbf{V}_\ell \in \mathbb{C}^{N_t \times d_\ell}$ for the signal of UE$_\ell$, the BS transmits the superimposed signal as $\mathbf{s} = \sum_{\ell=1}^{L} \mathbf{V}_\ell \, \mathbf{s}_\ell$, where $\mathbf{s}_\ell \in \mathbb{C}^{d_\ell \times 1}$ is d_ℓ data streams intended for UE$_\ell$. It can be generally assumed that $\mathbb{E}(\mathbf{s}_\ell \, \mathbf{s}_\ell^H) = \mathbf{I}_{d_\ell}$, $\mathbb{E}(\mathbf{s}_\ell \, \mathbf{s}_i^H) = \mathbf{0}$ for $\ell \neq i$. We denote the channel matrix from the BS to the IRS, from the IRS to UE$_\ell$, and from the BS to UE$_\ell$ by $\mathbf{G} \in \mathbb{C}^{N \times N_t}$, $\mathbf{H}_{r,\ell} \in \mathbb{C}^{N_r \times N}$, and $\mathbf{H}_{b,\ell} \in \mathbb{C}^{N_r \times N_t}$, respectively. Note that the channel state information (CSI) acquisition in IRS-aided WCSs is challenging due to the presence of a large number of passive reflecting elements at the IRS. The various channel estimation schemes for IRS-related channels were introduced in [22, 23]. To explore the achievable system performance, we consider the scenario where the BS has access to perfect CSI. Such assumption is widely adopted in related studies [5, 13, 14]. The interactions of the IRS elements with the impinging signals are represented by matrix $\mathbf{\Theta} = \text{diag}\,(\gamma_1\theta_1, \gamma_2\theta_2, \cdots, \gamma_N\theta_N)$ where $\theta_n = \mathrm{e}^{j\phi_n}$ for $n \in \mathcal{N} = \{1, \cdots, N\}$. For reflecting element n, $\gamma_n \in [0, 1]$ and $\phi_n \in (0, 2\pi]$ respectively represent its reflection amplitude and phase shift. For simplicity, we assume that $\gamma_n = 1, \forall n$ [3]. Define $\mathbf{H}_\ell \triangleq \mathbf{H}_{b,\ell} + \mathbf{H}_{r,\ell} \, \mathbf{\Theta} \, \mathbf{G}$ as the effective channel from the BS to UE$_\ell$. Then, the received signal at UE$_\ell$ can be written as

$$\mathbf{y}_\ell = \mathbf{H}_\ell \, \mathbf{V}_\ell \, \mathbf{s}_\ell + \sum_{i=1, i\neq\ell}^{L} \mathbf{H}_\ell \, \mathbf{V}_i \, \mathbf{s}_i + \mathbf{n}_{r_\ell}, \ \ell \in \mathcal{L}, \quad (1)$$

where $\mathbf{n}_{r_\ell} \sim \mathcal{CN}\left(\mathbf{0}, \sigma_{r_\ell}^2 \, \mathbf{I}_{N_r}\right)$ is additive white Gaussian noise (AWGN) at UE$_\ell$.

To facilitate EH, the PS circuits at the users are deployed to partition the received signals into two streams: one dedicated to ID and the other intended for EH. Denoting a PSR ρ_ℓ as the portion of the signal used for ID at UE$_\ell$, its signal for ID is given by

$$\mathbf{y}_{ID,\ell} = \sqrt{\rho_\ell} \, \mathbf{H}_\ell \, \mathbf{V}_\ell \, \mathbf{s}_\ell + \sqrt{\rho_\ell} \sum_{i=1, i\neq\ell}^{L} \mathbf{H}_\ell \, \mathbf{V}_i \, \mathbf{s}_i + \sqrt{\rho_\ell} \, \mathbf{n}_{r_\ell} + \mathbf{n}_{c_\ell}, \ \ell \in \mathcal{L}, \quad (2)$$

where $\mathbf{n}_{c_\ell} \sim \mathcal{CN}\left(\mathbf{0}, \sigma_{c_\ell}^2 \, \mathbf{I}_{N_r}\right)$ is additional noise caused by the ID circuits at UE$_\ell$ [24]. Accordingly, the achievable data rate for UE$_\ell$ is

$$\zeta_\ell(\mathbf{V}, \boldsymbol{\rho}, \boldsymbol{\theta}) = \log_2 \left| \mathbf{I}_{N_r} + \mathbf{H}_\ell \, \mathbf{V}_\ell \, \mathbf{V}_\ell^H \, \mathbf{H}_\ell^H \, \mathbf{J}_\ell^{-1} \right|, \quad (3)$$

where we have defined $\mathbf{V} = \{\mathbf{V}_1, \mathbf{V}_2, \ldots, \mathbf{V}_L\}$, $\boldsymbol{\theta} = [\theta_1, \theta_2, \ldots, \theta_N]^T$, $\boldsymbol{\rho} = [\rho_1, \rho_2, \ldots, \rho_L]^T$, and $\mathbf{J}_\ell = \sum_{i=1, i\neq\ell}^{L} \mathbf{H}_\ell \, \mathbf{V}_i \, \mathbf{V}_i^H \, \mathbf{H}_\ell^H + \sigma_{r_\ell}^2 \, \mathbf{I}_{N_r} + \rho_\ell^{-1} \sigma_{c_\ell}^2 \, \mathbf{I}_{N_r}$. From the received signal in (1), the remaining signal stream for EH at UE$_\ell$ is given by

$$\mathbf{y}_{EH,\ell} = \sqrt{1-\rho_\ell} \sum_{i=1}^{L} \mathbf{H}_\ell \, \mathbf{V}_i \, \mathbf{s}_i + \sqrt{1-\rho_\ell} \, \mathbf{n}_{r_\ell}, \ \ell \in \mathcal{L}. \quad (4)$$

Note that in practical scenarios, the noise power is significantly lower compared to the RF power, and therefore, it is ignored for EH. Then, the input energy of the EH circuits at the UE$_\ell$ is expressed as $\xi_\ell(\mathbf{V}, \boldsymbol{\rho}, \boldsymbol{\theta}) = (1-\rho_\ell) \, \text{Tr}\left(\sum_{i=1}^{L} \mathbf{H}_\ell \, \mathbf{V}_i \, \mathbf{V}_i^H \, \mathbf{H}_\ell^H\right)$. As shown in recent works [25, 26], the practical EH circuits exhibit a non-linear RF energy conversion. Specifically, the practical experiments show that for the lower input power the output power of the EH circuits increases but for the high input power, the output power becomes saturated at the maximum possible power. Thus, the assumption of linear EH models can lead to the system performance loss due to a mismatch between the practical EH models with the ideal linear EH ones. Accordingly, it is important to take practical NLEH models into consideration while designing the optimal transmission strategies. With adopting the NLEH model [25], the total HE at UE$_\ell$ can be obtained by

$$\xi_\ell^{NL}(\mathbf{V}, \boldsymbol{\rho}, \boldsymbol{\theta}) = \Gamma_\ell \left(1 + \mathrm{e}^{-a_\ell(\xi_\ell(\mathbf{V}, \boldsymbol{\rho}, \boldsymbol{\theta}) - b_\ell)}\right)^{-1} - \Gamma_\ell \mathrm{Y}_\ell. \quad (5)$$

Here, $\mathrm{Y}_\ell = 1/\left(1 + \mathrm{e}^{a_\ell b_\ell}\right)$, $\Gamma_\ell = P_\ell / \left(1 - \mathrm{Y}_\ell\right)$ where constants a_ℓ and b_ℓ are determined by the characteristics of electronic components in the EH circuits. Additionally, P_ℓ represents the maximum harvested power at UE$_\ell$ when the EH circuit attains saturation.

3 Multi-Objective Optimization Formulation

This paper aims to simultaneously maximize the SR and SHE at the users by optimally designing the BS TPMs, the IRS PSM, and the PSRs under the practical constraints imposed on the TP, the minimum data rate and HE. However, the objectives of the SRM and SHEM may conflict with each other [19]. Therefore, to study the insightful tradeoff between them, we formulate the design problem as a MOOP. To this end, we firstly

introduce two SOOPs, then we formulate a MOOP from those SOOPs.

3.1 SOOP for SRM Problem

The achievable bit rate of the system is key performance metric in the design and evaluation of WCSs. Thus, the first SOOP is to maximize the achievable SR of the system. The SRM problem can be represented as a minimization one

$$\text{SOOP 1}: \min_{\mathbf{V},\boldsymbol{\rho},\boldsymbol{\theta}} \quad \Omega_1(\mathbf{V},\boldsymbol{\rho},\boldsymbol{\theta}) \triangleq -\sum_{\ell=1}^{L} \zeta_\ell(\mathbf{V},\boldsymbol{\rho},\boldsymbol{\theta}) \quad (6a)$$

$$\text{s.t.} \quad \sum_{\ell=1}^{L} \mathsf{Tr}\left(\mathbf{V}_\ell \mathbf{V}_\ell^H\right) \le P_{max}, \quad (6b)$$

$$\zeta_\ell(\mathbf{V},\boldsymbol{\rho},\boldsymbol{\theta}) \ge \mathtt{r}_\ell^{req},\ \ell \in \mathcal{L}, \quad (6c)$$

$$\xi_\ell^{NL}(\mathbf{V},\boldsymbol{\rho},\boldsymbol{\theta}) \ge \mathtt{e}_\ell^{req},\ \ell \in \mathcal{L}, \quad (6d)$$

$$|\theta_n| = 1,\ n \in \mathcal{N}, \quad (6e)$$

$$0 \le \rho_\ell \le 1,\ \ell \in \mathcal{L}, \quad (6f)$$

where P_{max} is the maximum BS TP budget while $\mathtt{r}_\ell^{req}$ and $\mathtt{e}_\ell^{req}$ are the minimum user rate requirement and the minimum HE requirement at UE_ℓ, respectively. Constraint (6b) restricts the maximum TP at the BS. Constraint (6c) guarantees the QoS in terms of the achievable user rate for each user while constraint (6d) guarantees the minimum amount of HE for each users. Constraint (6e) imposes the unit-modulus on the IRS reflective elements.

3.2 SOOP for SHEM Problem

Apart from the performance metric of the SR, in SWIPT systems, maximizing the amount of HE is another desirable objective. Thus, the second SOOP aiming at the SHEM is formulated as

$$\text{SOOP 2}: \min_{\mathbf{V},\boldsymbol{\rho},\boldsymbol{\theta}} \quad \Omega_2(\mathbf{V},\boldsymbol{\rho},\boldsymbol{\theta}) \triangleq -\sum_{\ell=1}^{L} \xi_\ell^{NL}(\mathbf{V},\boldsymbol{\rho},\boldsymbol{\theta}) \quad (7a)$$

$$\text{s.t.} \quad (6b)-(6f). \quad (7b)$$

3.3 MOOP for the SRM and SHEM

Note that the objectives of the SRM in SOOP 1 and the SHEM in SOOP 2 are mutually conflicting. One solution to maximize the SR performance can result in the degradation in the SHE performance. Thus, the MOOP which aims at simultaneously optimizing both performance metrics is practically necessary. The MOOP is expressed as

$$\text{MOOP}: \min_{\mathbf{V},\boldsymbol{\rho},\boldsymbol{\theta}} \quad \Omega_3(\mathbf{V},\boldsymbol{\rho},\boldsymbol{\theta}) \quad (8a)$$

$$\text{s.t.} \quad (6b)-(6f). \quad (8b)$$

where $\Omega_3(\mathbf{V},\boldsymbol{\rho},\boldsymbol{\theta}) \triangleq [\Omega_1(\mathbf{V},\boldsymbol{\rho},\boldsymbol{\theta}), \Omega_2(\mathbf{V},\boldsymbol{\rho},\boldsymbol{\theta})]$ and the OFs in problems SOOP 1 and SOOP 2 are the elements of the OF vector in (8).

Due to the coupled variables of the TPMs, PSRs, and PSM, OFs in problems (6), (7), and (8) are highly non-linear and non-convex. Regarding the constraints, it is worth noting that the minimum user data rate constraints in (6c) are non-convex with respect to (w.r.t.) the design variables and the EH constraints in (6d) are more complicated and non-convex due to the NLEH models. Furthermore, the unit-modulus constraints on IRS reflective elements in (6e) pose a non-convex nature, which makes the OPs intractable to solve.

4 Proposed Method for SRM and SHEM

In this section, we employ the AO approach to decompose each original problem, namely SOOP 1, SOOP 2, and MOOP, into amenable sub-problems. Initially, we obtain the optimal TPMs and PSRs with fixed phase shifts. Subsequently, with fixed TPMs and PSRs, we determine the optimal phase shifts. In each sub-problem, in order to address non-convex OFs and non-convex constraints, we aim to identify suitable surrogate functions. This is achieved by applying the MM method to reformulate the design problems into convex optimization ones.

4.1 Proposed Method for SOOP of SRM

4.1.1 Joint Design of TPMs and PSRs: In this subsection, we fix $\boldsymbol{\theta}$ while the BS TPMs and the user PSRs are optimally designed. Then, problem (6) is rewritten as

$$\min_{\mathbf{V},\boldsymbol{\rho}} \quad \Omega_1(\mathbf{V},\boldsymbol{\rho}) \triangleq -\sum_{\ell=1}^{L} \zeta_\ell(\mathbf{V},\boldsymbol{\rho}) \quad (9a)$$

$$\text{s.t.} \quad \zeta_\ell(\mathbf{V},\boldsymbol{\rho}) \ge \mathtt{r}_\ell^{req},\ \ell \in \mathcal{L}, \quad (9b)$$

$$\xi_\ell^{NL}(\mathbf{V},\boldsymbol{\rho}) \ge \mathtt{e}_\ell^{req},\ \ell \in \mathcal{L}, \quad (9c)$$

$$(6b), (6f). \quad (9d)$$

We aim at finding the concave lower bound of non-convex $\zeta_\ell(\mathbf{V},\boldsymbol{\rho})$ in (9a) and (9b). To this end, at iteration m, we define $\mathbf{J}_\ell^{(m)} = \sum_{i=1, i\neq\ell}^{L} \mathbf{H}_\ell \mathbf{V}_i^{(m)} \mathbf{V}_i^{(m),H} \mathbf{H}_\ell^H + \sigma_{r_\ell}^2 \mathbf{I}_{N_r} + \rho_\ell^{(m),-1} \sigma_{c_\ell}^2 \mathbf{I}_{N_r}$, $\mathcal{C}_{B,\ell} = \frac{1}{\ln(2)} \mathbf{J}_\ell^{(m),-1} \mathbf{H}_\ell \mathbf{V}_\ell^{(m)}$, $c_{B,\ell} = \log_2\left|\mathbf{I}_{N_r} + \mathbf{H}_\ell \mathbf{V}_\ell^{(m)} \mathbf{V}_\ell^{(m),H} \mathbf{H}_\ell^H \mathbf{J}_\ell^{(m),-1}\right| - \frac{1}{\ln(2)} \mathsf{Tr}\left(\mathbf{V}_\ell^{(m),H} \mathbf{H}_\ell^H \mathbf{J}_\ell^{(m),-1} \mathbf{H}_\ell \mathbf{V}_\ell^{(m)}\right)$, $\mathcal{D}_{B,\ell} = \frac{1}{\ln(2)}(\mathbf{J}_\ell^{(m),-1} - (\mathbf{J}_\ell^{(m)} + \mathbf{H}_\ell \mathbf{V}_\ell^{(m)} \mathbf{V}_\ell^{(m),H} \mathbf{H}_\ell^H)^{-1}) \succeq \mathbf{0}$.

Then, the following inequality is hold [27]

$$\begin{aligned}\zeta_\ell(\mathbf{V},\boldsymbol{\rho}) \ge \tilde{\zeta}_\ell(\mathbf{V},\boldsymbol{\rho}) &= c_{B,\ell} \\ &+ 2\Re\left\{\mathsf{Tr}\left(\mathcal{C}_{B,\ell}^H \mathbf{H}_\ell \mathbf{V}_\ell\right)\right\} \\ &- \mathsf{Tr}\left(\mathcal{D}_{B,\ell}^H \left(\mathbf{H}_\ell \mathbf{V}_\ell \mathbf{V}_\ell^H \mathbf{H}_\ell^H + \mathbf{J}_\ell\right)\right). \end{aligned} \quad (10)$$

To deal with the non-convex constraint in (9c), we firstly transform it into an equivalent form as follows

$$\psi_\ell(\mathbf{V}) \triangleq \mathsf{Tr}\left(\sum_{i=1}^{L} \mathbf{H}_\ell \mathbf{V}_i \mathbf{V}_i^H \mathbf{H}_\ell^H\right) \ge \frac{\bar{\xi}_\ell}{(1-\rho_\ell)}, \quad (11)$$

where $\bar{\xi}_\ell \triangleq b_\ell - \frac{1}{a_\ell}\ln\left(\frac{\Gamma_\ell}{\mathtt{e}_\ell^{req} + \Gamma_\ell Y_\ell} - 1\right)$. Since $\psi_\ell(\mathbf{V})$ in (11) is convex w.r.t. $\mathbf{V}$ and, thus, its lower bound

is given by using its first-order Taylor expansion at $\mathbf{V}^{(m)}$ as [27]

$$\psi_\ell(\mathbf{V}) \geq \tilde{\psi}_\ell(\mathbf{V}) \triangleq 2\Re\left\{\mathsf{Tr}\left(\sum_{i=1}^{L}\mathbf{H}_\ell\,\mathbf{V}_i^{(m)}\,\mathbf{V}_i^H\,\mathbf{H}_\ell^H\right)\right\} - \mathsf{Tr}\left(\sum_{i=1}^{L}\mathbf{H}_\ell\,\mathbf{V}_i^{(m)}\,\mathbf{V}_i^{(m),H}\,\mathbf{H}_\ell^H\right). \quad (12)$$

Substituting (12) into (11) yields the inner convex approximation of (9c) as

$$\tilde{\psi}_\ell(\mathbf{V}) \geq \frac{\bar{\xi}_\ell}{(1-\rho_\ell)},\ \ell\in\mathcal{L}. \quad (13)$$

From the above discussion, problem (9) can be reformulated as

$$\min_{\mathbf{V},\boldsymbol{\rho}}\quad \tilde{\Omega}_1(\mathbf{V},\boldsymbol{\rho}) \triangleq -\sum_{\ell=1}^{L}\tilde{\zeta}_\ell(\mathbf{V},\boldsymbol{\rho}) \quad (14a)$$

$$\text{s.t.}\quad \tilde{\zeta}_\ell(\mathbf{V},\boldsymbol{\rho}) \geq \mathtt{r}_\ell^{req},\ \ell\in\mathcal{L}, \quad (14b)$$

$$(6b),(6f),(13). \quad (14c)$$

Now, problem (14) is jointly convex w.r.t. $\{\mathbf{V},\boldsymbol{\rho}\}$ and, thus, it can be efficiently solved by convex program solvers, e.g., CVX packages [28].

4.1.2 Design of the Phase Shifts: Next, we focus on optimizing $\boldsymbol{\theta}$ with given $\{\mathbf{V},\boldsymbol{\rho}\}$. Accordingly, problem (6) is rewritten as

$$\min_{\boldsymbol{\theta}}\quad \Omega_1(\boldsymbol{\theta}) \triangleq -\sum_{\ell=1}^{L}\zeta_\ell(\boldsymbol{\theta}) \quad (15a)$$

$$\text{s.t.}\quad \zeta_\ell(\boldsymbol{\theta}) \geq \mathtt{r}_\ell^{req},\ \forall\ell\in\mathcal{L}, \quad (15b)$$

$$\xi_\ell^{NL}(\boldsymbol{\theta}) \geq \mathtt{e}_\ell^{req},\ \forall\ell\in\mathcal{L}, \quad (15c)$$

$$(6e). \quad (15d)$$

Similar to (10), we derive the lower bound of $\zeta_\ell(\boldsymbol{\theta})$ as follows

$$\zeta_\ell(\boldsymbol{\theta}) \geq \tilde{\zeta}_\ell(\boldsymbol{\theta}) = c_{R,\ell} + 2\Re\left\{\mathsf{Tr}\left(\mathcal{C}_{R,\ell}^H\,\mathbf{H}_\ell\,\mathbf{V}_\ell\right)\right\} - \mathsf{Tr}\left(\sum_{i=1}^{L}\mathcal{D}_{R,\ell}^H\,\mathbf{H}_\ell\,\mathbf{V}_i\,\mathbf{V}_i^H\,\mathbf{H}_\ell^H\right) - \mathsf{Tr}\left(\mathcal{D}_{R,\ell}^H\left(\sigma_{r_\ell}^2+\rho_\ell^{-1}\sigma_{c_\ell}^2\right)\right), \quad (16)$$

where $c_{R,\ell} = \log_2\left|\mathbf{I}_{N_r} + \mathbf{H}_\ell^{(z)}\,\mathbf{V}_\ell\,\mathbf{V}_\ell^H\,\mathbf{H}_\ell^{(z),H}\,\mathbf{J}_\ell^{(z),-1}\right|$
$- \frac{1}{\ln(2)}\mathsf{Tr}\left(\mathbf{V}_\ell^H\,\mathbf{H}_\ell^{(z),H}\,\mathbf{J}_\ell^{(z),-1}\,\mathbf{H}_\ell^{(z)}\,\mathbf{V}_\ell\right)$, $\mathcal{C}_{R,\ell}$
$= \frac{1}{\ln(2)}\,\mathbf{J}_\ell^{(z),-1}\,\mathbf{H}_\ell^{(z)}\,\mathbf{V}_\ell$, $\mathcal{D}_{R,\ell}$
$= \frac{1}{\ln(2)}(\mathbf{J}_\ell^{(z),-1} - (\mathbf{J}_\ell^{(z)} + \mathbf{H}_\ell^{(z)}\,\mathbf{V}_\ell\,\mathbf{V}_\ell^H\,\mathbf{H}_\ell^{(z),H})^{-1}) \succeq \mathbf{0}$, $\mathbf{J}_\ell^{(z)}$
$= \sum_{i=1,i\neq\ell}^{L}\mathbf{H}_\ell^{(z)}\,\mathbf{V}_i\,\mathbf{V}_i^H\,\mathbf{H}_\ell^{(z),H} + \sigma_{r_\ell}^2\,\mathbf{I}_{N_r} + \rho_\ell^{-1}\sigma_{c_\ell}^2\,\mathbf{I}_{N_r}$,
$\mathbf{H}_\ell^{(z)} \triangleq \mathbf{H}_{b,\ell} + \mathbf{H}_{r,\ell}\,\boldsymbol{\Theta}^{(z)}\,\mathbf{G}$.

By substituting $\mathbf{H}_\ell \triangleq \mathbf{H}_{b,\ell} + \mathbf{H}_{r,\ell}\,\boldsymbol{\Theta}\,\mathbf{G}$ into (16) and using the matrix identity in [29, 30] that $\sum_{i=1}^{L}\mathsf{Tr}\left(\boldsymbol{\Theta}^H\,\mathbf{W}_\ell\,\boldsymbol{\Theta}\,\mathbf{Z}_i\right) = \sum_{i=1}^{L}\boldsymbol{\theta}^H\left(\mathbf{W}_\ell\odot\mathbf{Z}_i^T\right)\boldsymbol{\theta}$, where $\mathbf{W}_\ell = \mathbf{H}_{r,\ell}^H\,\mathcal{D}_{R,\ell}^H\,\mathbf{H}_{r,\ell}$, and $\mathbf{Z}_i = \mathbf{G}\,\mathbf{V}_i\,\mathbf{V}_i^H\,\mathbf{G}^H$, the lower bound $\tilde{\zeta}_\ell(\boldsymbol{\theta})$ in (16) can be expressed as

$$\begin{aligned}\tilde{\zeta}_\ell(\boldsymbol{\theta}) = {} & c_{R,\ell} + 2\Re\left\{\mathsf{Tr}\left(\mathcal{C}_{R,\ell}^H\left(\mathbf{H}_{b,\ell}+\mathbf{H}_{r,\ell}\,\boldsymbol{\Theta}\,\mathbf{G}\right)\mathbf{V}_\ell\right)\right\} \\ & - \mathsf{Tr}\left(\sum_{i=1}^{L}\mathbf{H}_{b,\ell}^H\,\mathcal{D}_{R,\ell}^H\,\mathbf{H}_{b,\ell}\,\mathbf{V}_i\,\mathbf{V}_i^H\right) \\ & - \mathsf{Tr}\left(\sum_{i=1}^{L}\mathbf{H}_{b,\ell}^H\,\mathcal{D}_{R,\ell}^H\,\mathbf{H}_{r,\ell}\,\boldsymbol{\Theta}\,\mathbf{G}\,\mathbf{V}_i\,\mathbf{V}_i^H\right) \\ & - \mathsf{Tr}\left(\sum_{i=1}^{L}\mathbf{G}^H\,\boldsymbol{\Theta}^H\,\mathbf{H}_{r,\ell}^H\,\mathcal{D}_{R,\ell}^H\,\mathbf{H}_{b,\ell}\,\mathbf{V}_i\,\mathbf{V}_i^H\right) \\ & - \sum_{i=1}^{L}\boldsymbol{\theta}^H\left(\mathbf{W}_\ell\odot\mathbf{Z}_i^T\right)\boldsymbol{\theta} \\ & - \mathsf{Tr}\left(\mathcal{D}_{R,\ell}^H\left(\sigma_{r_\ell}^2+\rho_\ell^{-1}\sigma_{c_\ell}^2\right)\right). \end{aligned} \quad (17)$$

Similar to (11), constraint (15c) can be rewritten w.r.t. $\boldsymbol{\theta}$ as follows

$$\psi_\ell(\boldsymbol{\theta}) \triangleq \mathsf{Tr}\left(\sum_{i=1}^{L}\mathbf{H}_\ell\,\mathbf{V}_i\,\mathbf{V}_i^H\,\mathbf{H}_\ell^H\right) \geq \frac{\bar{\xi}_\ell}{(1-\rho_\ell)}. \quad (18)$$

Similar to (12), the lower bound of $\psi_\ell(\boldsymbol{\theta})$ can be given by

$$\psi_\ell(\boldsymbol{\theta}) \geq \tilde{\psi}_\ell(\boldsymbol{\theta}) \triangleq 2\Re\left\{\mathsf{Tr}\left(\sum_{i=1}^{L}\mathbf{H}_\ell^{(z)}\,\mathbf{V}_i\,\mathbf{V}_i^H\,\mathbf{H}_\ell^H\right)\right\} - \mathsf{Tr}\left(\sum_{i=1}^{L}\mathbf{H}_\ell^{(z)}\,\mathbf{V}_i\,\mathbf{V}_i^H\,\mathbf{H}_\ell^{(z),H}\right). \quad (19)$$

To address non-convex constraint (6e), a relaxation and penalty approaches are employed. Constraint (6e) can be relaxed as follows [31, 32]

$$\begin{cases}|\theta_n|^2 \leq 1+\nu_n, \forall n\in\mathcal{N}, & (20a)\\ |\theta_n|^2 \geq 1-\mu_n, \forall n\in\mathcal{N}, & (20b)\end{cases}$$

with auxiliary variables $\mu_n \geq 0$ and $\nu_n \geq 0, \forall n\in\mathcal{N}$. To handle constraint (20b), we use its inner convex set at $\theta_n^{(z)}$ as [27, 33]

$$2\Re\left\{\theta_n^{(z),*}\theta_n\right\} - \left|\theta_n^{(z)}\right|^2 \geq 1-\mu_n, \forall n\in\mathcal{N}. \quad (21)$$

By denoting $\boldsymbol{\mu} = [\mu_1,\cdots,\mu_N]^T$, $\boldsymbol{\nu} = [\nu_1,\cdots,\nu_N]^T$ and applying the penalty method, problem (15) can be recast as

$$\min_{\boldsymbol{\theta},\boldsymbol{\mu},\boldsymbol{\nu}}\quad \tilde{\Omega}_1(\boldsymbol{\theta}) \triangleq -\sum_{\ell=1}^{L}\tilde{\zeta}_\ell(\boldsymbol{\theta}) + \beta\left(\sum_{n=1}^{N}\mu_n + \sum_{n=1}^{N}\nu_n\right) \quad (22a)$$

$$\text{s.t.}\quad \tilde{\zeta}_\ell(\boldsymbol{\theta}) \geq \mathtt{r}_\ell^{req},\ \ell\in\mathcal{L}, \quad (22b)$$

$$\tilde{\psi}_\ell(\boldsymbol{\theta}) \geq \frac{\bar{\xi}_\ell}{(1-\rho_\ell)},\ \ell\in\mathcal{L}, \quad (22c)$$

$$\mu_n\geq 0, \nu_n\geq 0, n\in\mathcal{N}, \quad (22d)$$

$$(20a),(21), \quad (22e)$$

where β is a penalty parameter. The penalty is involved in the OF in (22a) such that μ_n and ν_n approach to zero and, then, $|\theta_n|, \forall n\in\mathcal{N}$ reaches to 1. Note that the OP (22) is convex and its optimal solution can be obtained by standard convex solvers [28].

As a result, the iterative procedure for maximizing the SR of the users by alternatively updating the TPMs, PSRs, and PSM is presented in Algorithm 1 with the maximum number of iterations ϱ_{max} and error tolerance ε. Note that to facilitate the convergence of the iterative algorithm, the penalty parameter is updated at each iteration and is confined to a maximum value β_{max}.

Algorithm 1 An AO algorithm for the SRM

1: **Inputs**: Set ε and ϱ_{max}.
2: **Initialization**: feasible $\mathbf{V}^{(0)} = \mathbf{V}_*^{(0)}$, $\boldsymbol{\theta}^{(0)} = \boldsymbol{\theta}_*^{(0)}$ $\boldsymbol{\rho}^{(0)} = \boldsymbol{\rho}_*^{(0)}$, and set $r = 0$.
3: **repeat**
4: Set $m = 0$, $\mathbf{V}^{(m)} = \mathbf{V}_*^{(r)}$, $\boldsymbol{\rho}^{(m)} = \boldsymbol{\rho}_*^{(r)}$;
5: **repeat**
6: For given $\boldsymbol{\theta} = \boldsymbol{\theta}_*^{(r)}$, solve problem (14) to obtain the solutions $\tilde{\mathbf{V}}$ and $\tilde{\boldsymbol{\rho}}$;
7: Update $m \leftarrow m+1, \mathbf{V}^{(m)} = \tilde{\mathbf{V}}, \boldsymbol{\rho}^{(m)} = \tilde{\boldsymbol{\rho}}$;
8: **until** $\frac{\left|\tilde{\Omega}_1(\mathbf{V}^{(m)},\boldsymbol{\rho}^{(m)}) - \tilde{\Omega}_1(\mathbf{V}^{(m-1)},\boldsymbol{\rho}^{(m-1)})\right|}{\tilde{\Omega}_1(\mathbf{V}^{(m-1)},\boldsymbol{\rho}^{(m-1)})} \leq \varepsilon$ or $m > \varrho_{max}$;
9: Obtain $\mathbf{V} = \tilde{\mathbf{V}}$, $\boldsymbol{\rho} = \tilde{\boldsymbol{\rho}}$;
10: Set $\beta > 0$, $\beta_{max} > 0$, $\delta > 1$, $z = 0$, $\boldsymbol{\theta}^{(z)} = \boldsymbol{\theta}_*^{(r)}$;
11: **repeat**
12: For given $\mathbf{V}, \boldsymbol{\rho}$, solve problem (22) to obtain $\tilde{\boldsymbol{\theta}}$;
13: Update $z \leftarrow z+1$, $\beta = \min(\delta\beta, \beta_{max})$, $\boldsymbol{\theta}^{(z)} = \tilde{\boldsymbol{\theta}}$;
14: **until** $\frac{\left|\tilde{\Omega}_1(\boldsymbol{\theta}^{(z)}) - \tilde{\Omega}_1(\boldsymbol{\theta}^{(z-1)})\right|}{\tilde{\Omega}_1(\boldsymbol{\theta}^{(z-1)})} \leq \varepsilon$ or $z > \varrho_{max}$;
15: Obtain $\boldsymbol{\theta} = \tilde{\boldsymbol{\theta}}$;
16: Update $r \leftarrow r+1$, $\mathbf{V}_*^{(r)} = \mathbf{V}, \boldsymbol{\rho}_*^{(r)} = \boldsymbol{\rho}, \boldsymbol{\theta}_*^{(r)} = \boldsymbol{\theta}$;
17: **until** $\frac{\left|\tilde{\Omega}_1(\mathbf{V}_*^{(r)},\boldsymbol{\rho}_*^{(r)},\boldsymbol{\theta}_*^{(r)}) - \tilde{\Omega}_1(\mathbf{V}_*^{(r-1)},\boldsymbol{\rho}_*^{(r-1)},\boldsymbol{\theta}_*^{(r-1)})\right|}{\tilde{\Omega}_1(\mathbf{V}_*^{(r-1)},\boldsymbol{\rho}_*^{(r-1)},\boldsymbol{\theta}_*^{(r-1)})} < \varepsilon$ or $r > \varrho_{max}$;
18: **Outputs**: $\mathbf{V}^{(opt)} = \mathbf{V}_*^{(r)}, \boldsymbol{\rho}^{(opt)} = \boldsymbol{\rho}_*^{(r)}, \boldsymbol{\theta}^{(opt)} = \boldsymbol{\theta}_*^{(r)}$.

4.2 Proposed Method for SOOP of SHEM

4.2.1 Joint Design of TPMs and PSRs: Similar to Subsection 4.1.1, by fixing $\boldsymbol{\theta}$, problem (7) can be rewritten w.r.t. $\mathbf{V}$ and $\boldsymbol{\rho}$ as

$$\min_{\mathbf{V},\boldsymbol{\rho}} \quad \Omega_2(\mathbf{V},\boldsymbol{\rho}) \triangleq -\sum_{\ell=1}^{L} \xi_\ell^{NL}(\mathbf{V},\boldsymbol{\rho}) \tag{23a}$$

$$\text{s.t.} \quad (6b), (6f), (9b), (9c). \tag{23b}$$

In problem (23), constraints (9b), (9c) are handled in Subsection 4.1.1 and, thus we focus on handling the non-convex OF. To this end, we introduce auxiliary variables $\boldsymbol{\vartheta} \triangleq \{\vartheta_1, \vartheta_2, \cdots, \vartheta_L\}$ satisfying

$$\left(1 + \mathrm{e}^{-a_\ell(\xi_\ell(\mathbf{V},\boldsymbol{\rho}) - b_\ell)}\right)^{-1} - \Upsilon_\ell \geq \vartheta_\ell, \ell \in \mathcal{L}. \tag{24}$$

Then, the OF is lower-bounded by [34]

$$\xi_\ell^{NL}(\mathbf{V},\boldsymbol{\rho}) \geq \Gamma_\ell \vartheta_\ell, \ell \in \mathcal{L}. \tag{25}$$

By denoting $\boldsymbol{\lambda} \triangleq \{\lambda_1, \lambda_2, \cdots, \lambda_L\}$, inequality (24) can be recast as

$$\begin{cases} 1 - \Upsilon_\ell - \Upsilon_\ell\lambda_\ell - \vartheta_\ell \geq \lambda_\ell\vartheta_\ell, \ell \in \mathcal{L}, & (26a) \\ \xi_\ell(\mathbf{V},\boldsymbol{\rho}) + a_\ell^{-1}\ln(\lambda_\ell) \geq b_\ell, \ell \in \mathcal{L}. & (26b) \end{cases}$$

To handle non-convex constraints in (26a), we adopt Lemma 2 in [34] to find the upper bound of $\lambda_\ell\vartheta_\ell$ at given $\lambda_\ell^{(m)}$ and $\vartheta_\ell^{(m)}$ at iteration m as follows

$$\begin{aligned} \varphi(\lambda_\ell, \vartheta_\ell) &\triangleq 0.5\left(\lambda_\ell^{(m)}\vartheta_\ell^{(m),-1}\vartheta_\ell^2 + \vartheta_\ell^{(m)}\lambda_\ell^{(m),-1}\lambda_\ell^2\right) \\ &\geq \lambda_\ell\vartheta_\ell. \end{aligned} \tag{27}$$

Then, constraints in (26a) can be expressed as convex ones

$$1 - \Upsilon_\ell - \Upsilon_\ell\lambda_\ell - \vartheta_\ell \geq \varphi(\lambda_\ell, \vartheta_\ell), \ \ell \in \mathcal{L}. \tag{28}$$

Next, to tackle non-convex constraint (26b), we utilize the following inequality [35]

$$\begin{aligned} \mathbf{Y}^H\mathbf{X}^{-1}\mathbf{Y} \succeq\ & \mathbf{Y}^{(m),H}\mathbf{X}^{(m),-1}\mathbf{Y} + \mathbf{Y}^H\mathbf{X}^{(m),-1}\mathbf{Y}^{(m)} \\ & - \mathbf{Y}^{(m),H}\mathbf{X}^{(m),-1}\mathbf{X}\mathbf{X}^{(m),-1}\mathbf{Y}^{(m)}, \\ & \forall \mathbf{Y}, \mathbf{Y}^{(m)}, \ \mathbf{X} \succ \mathbf{0}, \ \mathbf{X}^{(m)} \succ \mathbf{0}. \end{aligned} \tag{29}$$

Accordingly, the lower bound of $\xi_\ell(\mathbf{V},\boldsymbol{\rho}) = \mathsf{Tr}\left(\sum_{i=1}^{L}(\mathbf{H}_\ell\mathbf{V}_i)^H\mathbf{X}_\ell^{-1}\mathbf{H}_\ell\mathbf{V}_i\right)$ with given $\rho_\ell^{(m)}$ and $\mathbf{V}_i^{(m)}$ at iteration m can be determined as

$$\begin{aligned} \xi_\ell(\mathbf{V},\boldsymbol{\rho}) \geq\ & \mathsf{Tr}\left(\sum_{i=1}^{L}\left(\mathbf{H}_\ell\mathbf{V}_i^{(m)}\right)^H\mathbf{X}_\ell^{(m),-1}\mathbf{H}_\ell\mathbf{V}_i\right) \\ & + \mathsf{Tr}\left(\sum_{i=1}^{L}(\mathbf{H}_\ell\mathbf{V}_i)^H\mathbf{X}_\ell^{(m),-1}\mathbf{H}_\ell\mathbf{V}_i^{(m)}\right) \\ & - \mathsf{Tr}\left(\sum_{i=1}^{L}\left(\mathbf{H}_\ell\mathbf{V}_i^{(m)}\right)^H\mathbf{X}_\ell^{(m),-1}\mathbf{X}_\ell\mathbf{X}_\ell^{(m),-1}\mathbf{H}_\ell\mathbf{V}_i^{(m)}\right) \\ & \triangleq \tilde{\xi}_\ell(\mathbf{V},\boldsymbol{\rho}), \end{aligned} \tag{30}$$

where $\mathbf{X}_\ell^{-1} = (1-\rho_\ell)\mathbf{I}_{N_r}$ and $\mathbf{X}_\ell^{(m),-1} = (1-\rho_\ell^{(m)})\mathbf{I}_{N_r}$. Then, constraint (26b) can be reformulated as the convex constraint as follows

$$\tilde{\xi}_\ell(\mathbf{V},\boldsymbol{\rho}) + a_\ell^{-1}\ln(\lambda_\ell) \geq b_\ell, \forall \ell \in \mathcal{L}. \tag{31}$$

From the above discussion, the design problem (23) w.r.t. variables $\{\mathbf{V},\boldsymbol{\rho}\}$ is recast as

$$\min_{\mathbf{V},\boldsymbol{\rho},\boldsymbol{\vartheta},\boldsymbol{\lambda}} \quad \tilde{\Omega}_2(\mathbf{V},\boldsymbol{\rho}) \triangleq -\sum_{\ell=1}^{L}\Gamma_\ell\vartheta_\ell \tag{32a}$$

$$\text{s.t.} \quad (6b), (6f), (13), (14b), (28), (31). \tag{32b}$$

Problem (32) is to minimize the linear OF over the convex constraints. Thus, its optimal solution can be efficiently obtained by the CVX packages [28].

4.2.2 Design of the Phase Shifts: Similar to Subsection 4.1.2, problem (7) can be expressed w.r.t. the variables $\boldsymbol{\theta}$ as

$$\min_{\boldsymbol{\theta}} \quad \Omega_2(\boldsymbol{\theta}) \triangleq -\sum_{\ell=1}^{L}\xi_\ell^{NL}(\boldsymbol{\theta}) \ \text{s.t.} \ (6e), (15b), (15c). \tag{33}$$

Considering the non-concave function $\xi_\ell^{NL}(\boldsymbol{\theta})$, we can derive its lower bound with the same approach in (25) as follows

$$\xi_\ell^{NL}(\boldsymbol{\theta}) \geq \Gamma_\ell\vartheta_\ell, \forall \ell \in \mathcal{L} \tag{34}$$

with additional constraints in (28) and

$$(1-\rho_\ell)\,\tilde{\psi}_\ell(\boldsymbol{\theta}) + a_\ell^{-1}\ln(\lambda_\ell) \geq b_\ell. \tag{35}$$

where $\tilde{\psi}_\ell(\boldsymbol{\theta})$ is determined as (19). Accordingly, problem (33) can be reformulated as

$$\min_{\boldsymbol{\theta},\boldsymbol{\vartheta},\boldsymbol{\lambda},\boldsymbol{\mu},\boldsymbol{\nu}} \quad \tilde{\Omega}_2(\boldsymbol{\theta}) \triangleq -\sum_{\ell=1}^{L}\Gamma_\ell\vartheta_\ell + \beta\left(\sum_{n=1}^{N}\mu_n + \sum_{n=1}^{N}\nu_n\right) \tag{36a}$$

$$\text{s.t.} \quad (22b), (22c), (22d), (20a), (21), (28), (35), \tag{36b}$$

whose optimal solutions can be efficiently obtained by convex optimization solvers.

Finally, the details of the iterative algorithm to alternatively obtain the BS TPMs, PSRs and PSM to optimize the SHE are represented in Algorithm 2.

Algorithm 2 An AO algorithm for the SHEM

1: **Inputs**: Set ε and ϱ_{max}.
2: **Initialization**: feasible $\mathbf{V}^{(0)} = \mathbf{V}_*^{(0)}$, $\boldsymbol{\theta}^{(0)} = \boldsymbol{\theta}_*^{(0)}$ $\boldsymbol{\rho}^{(0)} = \boldsymbol{\rho}_*^{(0)}$, and set $r = 0$.
3: **repeat**
4: Set $m = 0$, $\mathbf{V}^{(m)} = \mathbf{V}_*^{(r)}$, $\boldsymbol{\rho}^{(m)} = \boldsymbol{\rho}_*^{(r)}$;
5: **repeat**
6: For given $\boldsymbol{\theta} = \boldsymbol{\theta}_*^{(r)}$, solve problem (32) to obtain the solutions $\tilde{\mathbf{V}}$ and $\tilde{\boldsymbol{\rho}}$;
7: Update $m \leftarrow m+1, \mathbf{V}^{(m)} = \tilde{\mathbf{V}}, \boldsymbol{\rho}^{(m)} = \tilde{\boldsymbol{\rho}}$;
8: **until** $\frac{\left|\tilde{\Omega}_2(\mathbf{V}^{(m)},\boldsymbol{\rho}^{(m)}) - \tilde{\Omega}_2(\mathbf{V}^{(m-1)},\boldsymbol{\rho}^{(m-1)})\right|}{\tilde{\Omega}_2(\mathbf{V}^{(m-1)},\boldsymbol{\rho}^{(m-1)})} \le \varepsilon$ or $m > \varrho_{max}$;
9: Obtain $\mathbf{V} = \tilde{\mathbf{V}}$, $\boldsymbol{\rho} = \tilde{\boldsymbol{\rho}}$;
10: Set $\beta > 0$, $\beta_{max} > 0$, $\delta > 1$, $z = 0$, $\boldsymbol{\theta}^{(z)} = \boldsymbol{\theta}_*^{(r)}$;
11: **repeat**
12: For given $\mathbf{V}, \boldsymbol{\rho}$, solve problem (36) to obtain $\tilde{\boldsymbol{\theta}}$;
13: Update $z \leftarrow z+1$, $\beta = \min(\delta\beta, \beta_{max})$, $\boldsymbol{\theta}^{(z)} = \tilde{\boldsymbol{\theta}}$;
14: **until** $\frac{\left|\tilde{\Omega}_2(\boldsymbol{\theta}^{(z)}) - \tilde{\Omega}_2(\boldsymbol{\theta}^{(z-1)})\right|}{\tilde{\Omega}_2(\boldsymbol{\theta}^{(z-1)})} \le \varepsilon$ or $z > \varrho_{max}$;
15: Obtain $\boldsymbol{\theta} = \tilde{\boldsymbol{\theta}}$;
16: Update $r \leftarrow r+1$, $\mathbf{V}_*^{(r)} = \mathbf{V}, \boldsymbol{\rho}_*^{(r)} = \boldsymbol{\rho}, \boldsymbol{\theta}_*^{(r)} = \boldsymbol{\theta}$;
17: **until** $\frac{\left|\tilde{\Omega}_2(\mathbf{V}_*^{(r)},\boldsymbol{\rho}_*^{(r)},\boldsymbol{\theta}_*^{(r)}) - \tilde{\Omega}_2(\mathbf{V}_*^{(r-1)},\boldsymbol{\rho}_*^{(r-1)},\boldsymbol{\theta}_*^{(r-1)})\right|}{\tilde{\Omega}_2(\mathbf{V}_*^{(r-1)},\boldsymbol{\rho}_*^{(r-1)},\boldsymbol{\theta}_*^{(r-1)})} < \varepsilon$ or $r > \varrho_{max}$;
18: **Outputs**: $\mathbf{V}^{(opt)} = \mathbf{V}_*^{(r)}, \boldsymbol{\rho}^{(opt)} = \boldsymbol{\rho}_*^{(r)}, \boldsymbol{\theta}^{(opt)} = \boldsymbol{\theta}_*^{(r)}$.

4.3 Proposed Method for MOOP of SRM and SHEM

It is very difficult to jointly find the optimal solution to (8). To tackle it, we transform the MOOP of the SRM and SHEM into a SOOP by using the MWT method [21]. Given Ω_1^* and Ω_2^* which are respectively the optimal values of SOOP 1 and SOOP 2, the MOOP in (8) can be recast as

$$\min_{\mathbf{V},\boldsymbol{\rho},\boldsymbol{\theta}} \Omega_3(\mathbf{V},\boldsymbol{\rho},\boldsymbol{\theta}) \triangleq \max_{p\in\{1,2\}} \omega_p\left[\frac{\Omega_p(\mathbf{V},\boldsymbol{\rho},\boldsymbol{\theta}) - \Omega_p^*}{\left|\Omega_p^*\right|} + \tau\sum_{q\in\{1,2\}}\frac{\Omega_q(\mathbf{V},\boldsymbol{\rho},\boldsymbol{\theta}) - \Omega_q^*}{\left|\Omega_q^*\right|}\right] \tag{37a}$$

$$\text{s.t. } (6b) - (6f), \tag{37b}$$

where τ is a sufficiently small positive scalar which is normally chosen between 0.0001 and 0.01 [21]. The weighted parameters $\omega_p \in [0,1]$ with $\omega_1 + \omega_2 = 1$ can be set to the different values to investigate the tradeoffs between the achievable SR and achievable SHE.

4.3.1 Joint Design of TPMs and PSRs: Problem (37) can be recast w.r.t. $\mathbf{V}$ and $\boldsymbol{\rho}$ as follows

$$\min_{\mathbf{V},\boldsymbol{\rho}} \Omega_3(\mathbf{V},\boldsymbol{\rho}) \triangleq \max_{p\in\{1,2\}} \omega_p\left[\frac{\Omega_p(\mathbf{V},\boldsymbol{\rho}) - \Omega_p^*}{\left|\Omega_p^*\right|} + \tau\sum_{q\in\{1,2\}}\frac{\Omega_q(\mathbf{V},\boldsymbol{\rho}) - \Omega_q^*}{\left|\Omega_q^*\right|}\right] \tag{38a}$$

$$\text{s.t. } (6b), (6f), (9b), (9c). \tag{38b}$$

By introducing slack variable η, problem (38) can be equivalently expressed as

$$\min_{\substack{\mathbf{V},\boldsymbol{\rho},\boldsymbol{\vartheta},\\ \boldsymbol{\lambda},\eta}} \tilde{\Omega}_3(\mathbf{V},\boldsymbol{\rho}) \triangleq \eta \tag{39a}$$

$$\text{s.t. } (6b), (6f), (13), (14b), (28), (31), \tag{39b}$$

$$\frac{1+\tau}{|\Omega_1^*|}\tilde{\Omega}_1(\mathbf{V},\boldsymbol{\rho}) + \frac{\tau}{|\Omega_2^*|}\tilde{\Omega}_2(\mathbf{V},\boldsymbol{\rho}) \le \frac{\eta}{\omega_1} - 1 - 2\tau, \tag{39c}$$

$$\frac{\tau}{|\Omega_1^*|}\tilde{\Omega}_1(\mathbf{V},\boldsymbol{\rho}) + \frac{1+\tau}{|\Omega_2^*|}\tilde{\Omega}_2(\mathbf{V},\boldsymbol{\rho}) \le \frac{\eta}{\omega_2} - 1 - 2\tau, \tag{39d}$$

which is a convex optimization and can be solved by available convex optimization solvers.

4.3.2 Design of the Phase Shifts: This subsection aims to find the optimal IRS PSM. To end this, we solve the following problem

$$\min_{\boldsymbol{\theta}} \Omega_3(\boldsymbol{\theta}) \triangleq \max_{p\in\{1,2\}} \omega_p\left[\frac{\Omega_p(\boldsymbol{\theta}) - \Omega_p^*}{\left|\Omega_p^*\right|} + \tau\sum_{q\in\{1,2\}}\frac{\Omega_q(\boldsymbol{\theta}) - \Omega_q^*}{\left|\Omega_q^*\right|}\right] \tag{40a}$$

$$\text{s.t. } (6e), (15b), (15c). \tag{40b}$$

Similar to Subsection 4.3.1, problem (40) can be recast as a convex OP

$$\min_{\substack{\boldsymbol{\theta},\boldsymbol{\vartheta},\boldsymbol{\lambda},\\ \boldsymbol{\mu},\boldsymbol{\nu},\eta}} \tilde{\Omega}_3(\boldsymbol{\theta}) \triangleq \eta + \beta\left(\sum_{n=1}^{N}\mu_n + \sum_{n=1}^{N}\nu_n\right) \tag{41a}$$

$$\text{s.t. } (20a), (21), (22b), (22c), (22d), (28), (35), \tag{41b}$$

$$\frac{1+\tau}{|\Omega_1^*|}\tilde{\Omega}_1(\boldsymbol{\theta}) + \frac{\tau}{|\Omega_2^*|}\tilde{\Omega}_2(\boldsymbol{\theta}) \le \frac{\eta}{\omega_1} - 1 - 2\tau, \tag{41c}$$

$$\frac{\tau}{|\Omega_1^*|}\tilde{\Omega}_1(\boldsymbol{\theta}) + \frac{1+\tau}{|\Omega_2^*|}\tilde{\Omega}_2(\boldsymbol{\theta}) \le \frac{\eta}{\omega_2} - 1 - 2\tau, \tag{41d}$$

which can be efficiently solved by convex optimization solvers.

By solving the convex OPs in (39) and (41), the iterative algorithm to find the optimal TPMs, PSRs and PSM is described in Algorithm 3.

It is important to mention that in Algorithms 1, 2 and 3, each sub-problem is convex and, thus, its OF

Algorithm 3 An AO algorithm for the MOOP

Inputs: Set ε and ϱ_{max}.
Initialization: feasible $\mathbf{V}^{(0)} = \mathbf{V}_*^{(0)}$, $\boldsymbol{\theta}^{(0)} = \boldsymbol{\theta}_*^{(0)}$ $\boldsymbol{\rho}^{(0)} = \boldsymbol{\rho}_*^{(0)}$, and set $r = 0$.
Set weighted parameter sets ω_1 and $\omega_2 = 1 - \omega_1$;
repeat
  Set $m = 0$, $\mathbf{V}^{(m)} = \mathbf{V}_*^{(r)}$, $\boldsymbol{\rho}^{(m)} = \boldsymbol{\rho}_*^{(r)}$;
  repeat
    For given $\boldsymbol{\theta} = \boldsymbol{\theta}_*^{(r)}$, solve problem (39) to obtain the solutions $\tilde{\mathbf{V}}$ and $\tilde{\boldsymbol{\rho}}$;
    Update $m \leftarrow m+1, \mathbf{V}^{(m)} = \tilde{\mathbf{V}}, \boldsymbol{\rho}^{(m)} = \tilde{\boldsymbol{\rho}}$;
  until $\frac{\left|\tilde{\Omega}_3(\mathbf{V}^{(m)},\boldsymbol{\rho}^{(m)}) - \tilde{\Omega}_3(\mathbf{V}^{(m-1)},\boldsymbol{\rho}^{(m-1)})\right|}{\tilde{\Omega}_3(\mathbf{V}^{(m-1)},\boldsymbol{\rho}^{(m-1)})} \leq \varepsilon$ or $m > \varrho_{max}$;
  Obtain $\mathbf{V} = \tilde{\mathbf{V}}$, $\boldsymbol{\rho} = \tilde{\boldsymbol{\rho}}$;
  Set $\beta > 0$, $\beta_{max} > 0$, $\delta > 1$, $z = 0$, $\boldsymbol{\theta}^{(z)} = \boldsymbol{\theta}_*^{(r)}$;
  repeat
    For given $\mathbf{V}, \boldsymbol{\rho}$, solve problem (41) to obtain $\tilde{\boldsymbol{\theta}}$;
    Update $z \leftarrow z+1$, $\beta = \min(\delta\beta, \beta_{max})$, $\boldsymbol{\theta}^{(z)} = \tilde{\boldsymbol{\theta}}$;
  until $\frac{\left|\tilde{\Omega}_3(\boldsymbol{\theta}^{(z)}) - \tilde{\Omega}_3(\boldsymbol{\theta}^{(z-1)})\right|}{\tilde{\Omega}_3(\boldsymbol{\theta}^{(z-1)})} \leq \varepsilon$ or $z > \varrho_{max}$;
  Obtain $\boldsymbol{\theta} = \tilde{\boldsymbol{\theta}}$;
  Update $r \leftarrow r+1$, $\mathbf{V}_*^{(r)} = \mathbf{V}, \boldsymbol{\rho}_*^{(r)} = \boldsymbol{\rho}, \boldsymbol{\theta}_*^{(r)} = \boldsymbol{\theta}$;
until $\frac{\left|\tilde{\Omega}_3(\mathbf{V}_*^{(r)},\boldsymbol{\rho}_*^{(r)},\boldsymbol{\theta}_*^{(r)}) - \tilde{\Omega}_3(\mathbf{V}_*^{(r-1)},\boldsymbol{\rho}_*^{(r-1)},\boldsymbol{\theta}_*^{(r-1)})\right|}{\tilde{\Omega}_3(\mathbf{V}_*^{(r-1)},\boldsymbol{\rho}_*^{(r-1)},\boldsymbol{\theta}_*^{(r-1)})} < \varepsilon$ or $r > \varrho_{max}$;
Outputs: $\mathbf{V}^{(opt)} = \mathbf{V}_*^{(r)}, \boldsymbol{\rho}^{(opt)} = \boldsymbol{\rho}_*^{(r)}, \boldsymbol{\theta}^{(opt)} = \boldsymbol{\theta}_*^{(r)}$.

is not increasing over iterations. Therefore, the convergence of the AO algorithms is guaranteed since the OFs are non-increasing and lower-bounded. On the other hand, the computational complexity of Algorithms 1, 2 and 3 is polynomial-time since their solutions are obtained by convex optimization.

5 Numerical Results

The numerical simulations are conducted to assess the proposed methods and to investigate the tradeoff between achievable SR and SHE in the IRS-aided multi-user MIMO SWIPT system. We examine a scenario in which the BS is positioned at $(0, 2)$ meters and the IRS is deployed at $(3, 4)$ meters while $L = 3$ users are randomly located in a circle centered at $(5, 2)$ meters with radius 2 meters [5, 36]. The BS, which has $N_t = 4$ antennas, sends $d_\ell = 2, \forall \ell \in \mathcal{L}$ data streams to each user equipped with $N_r = 2$ antennas. The path loss between two nodes with the transmission distance x is modeled as $PL = PL_0 (x/x_0)^{-\alpha}$, where α represents the path loss exponent, $PL_0 = 10^{-3}$ denotes the path loss at the reference distance $x_0 = 1$ meter [5]. We examine scenarios where direct links from the BS to users encounter deep fading and shadowing. Consequently, the path loss exponents for these channels are set to $\alpha_{BU} = 3.75$. Simultaneously, to enhance signal transmission from the BS to users, the IRS is strategically positioned, ensuring that the line-of-sight paths from the BS to the IRS and from the IRS to users are predominant. Consequently, the path loss exponents for the channels from the BS to the IRS and from the IRS to users are respectively set to $\alpha_{BI} = 2.2$ and $\alpha_{IU} = 2.2$ [30]. The small-scale fading channels from the BS to the users adhere to the Rayleigh distribution while the other channels conform to the Rician distribution with a Rician factor of 3 [5]. The noise power is set $\sigma_{r_\ell}^2 = \sigma_{c_\ell}^2 = -60$ dBm, $\forall \ell \in \mathcal{L}$ [27]. The initial penalty parameter, the maximum penalty parameter, and the update step are set $\beta = 10$, $\beta_{max} = 1000$, and $\delta = 5$, respectively. Unless otherwise stated, we set $N = 30$, $\mathrm{e}_\ell^{req} = 0.01$ mW, $\mathrm{r}_\ell^{req} = 1$ bps/Hz, $P_\ell = 24$ mW, $a_\ell = 150, b_\ell = 0.014$, $\forall \ell \in \mathcal{L}$ [26]. Regarding the iterative algorithm, we set $\varrho_{max} = 100$ and $\varepsilon = 10^{-3}$. The numerical results are obtained by averaging over 100 random channel realizations.

Example 1: We investigate the convergence behaviour of the proposed MOOP algorithm under a specific channel realization with the maximum TP $P_{max} = 40$ dBm and different values of ω_1 in Figure 2. It is observed that the proposed MOOP algorithm reaches the convergence within 50 iterations. The results in Figure 2 also reveal that the convergence of MOOP can be reached faster for the smaller value of ω_1. The reason is that with the smaller values of ω_1, the MOOP prioritizes to optimize the SHE in the OF in which the OF of the SHE is approximated by a linear function and, thus, the optimal solution can be obtained efficiently. Additionally, Figure 3 depicts the evolution of the achievable SR and SHE of the SOOPs and the MOOP algorithm under a specific channel realization, respectively. It can be seen that the achievable SR and SHE are simultaneously non-decreasing over iterations. Moreover, since the MOOP have to ensure the tradeoff between the SR and SHE, the optimal values obtained by the MOOP with different quantities of ω_1 are always lower than the values of the corresponding SOOPs.

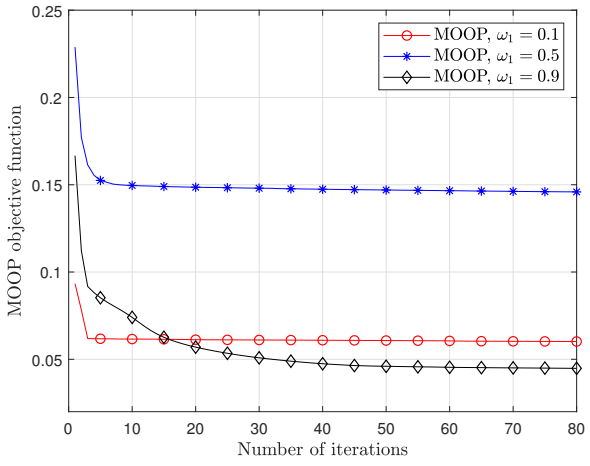

Figure 2. Convergence behaviour of the MOOP algorithm.

Example 2: This example evaluates the average achievable SR by using Algorithm 1 to solve SOOP 1 and the achievable SHE of all users by applying Algorithm 2 to solve SOOP 2 under different maximum TP levels of the BS. In addition to our approach, namely "Optimal

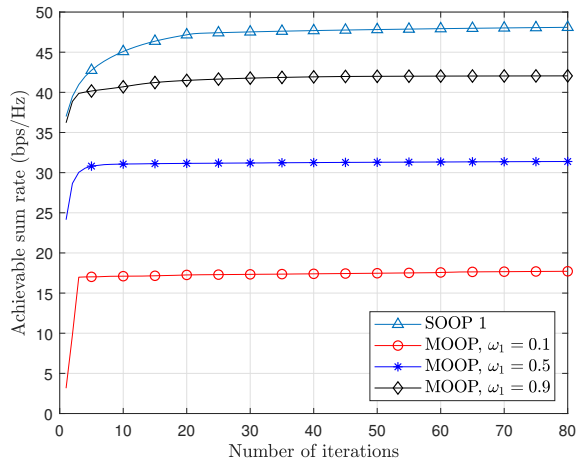

(a)

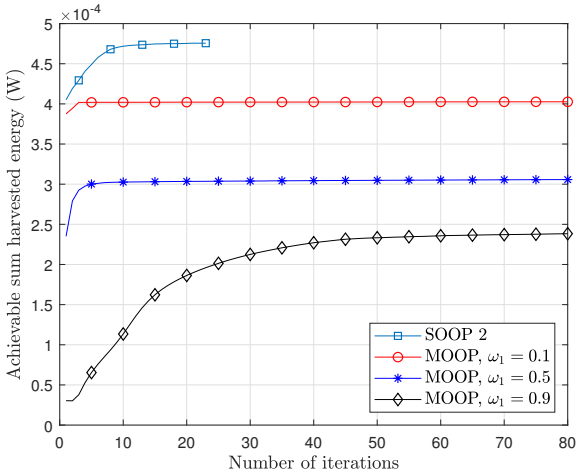

(b)

Figure 3. Achievable SR and SHE of the MOOP and SOOP algorithms.

phase", in which the TPMs, PSRs, and phase shifts are alternately optimized, we also consider two benchmark schemes, namely “Fixed phase" and “No-IRS", for comparison. For the fixed phase schemes, the phases of reflection element are fixed to be zero [13, 30]. For the No-IRS schemes, there is no IRS in the system. Figure 4 shows that the achievable SR and the achievable SHE of all considered schemes increase with P_{max}. However, the optimal phase schemes significantly outperform the other schemes. This is because for the optimal phase schemes the phase shifts at the IRS are optimized to create favourable effective transmission environments to improve the system performance in terms of the HE and achievable rate at all users. Moreover, the results indicate that the system performance in terms of the achievable SR and the achievable SHE with the fixed phase schemes is not much better than No-IRS schemes. Thus, optimizing the IRS phase shifts in a MU-MIMO SWIPT system assisted by the IRS is crucial for the system performance improvement. One interesting observation from Figure 4 is that as the TP exceeds 40 dBm the increase of the SR tends to be slower, while the increase in the achievable SHE becomes more pronounced. This is because that, for the SRM as shown in Figure 4(a), when the TP increases the co-channel interference also increases. On the contrary, for the SHEM as shown in Figure 4(b), as the TP increases the minimum user data rate and HE constraints are easily satisfied, and then the TP is maximally exploited to maximize the sum EH.

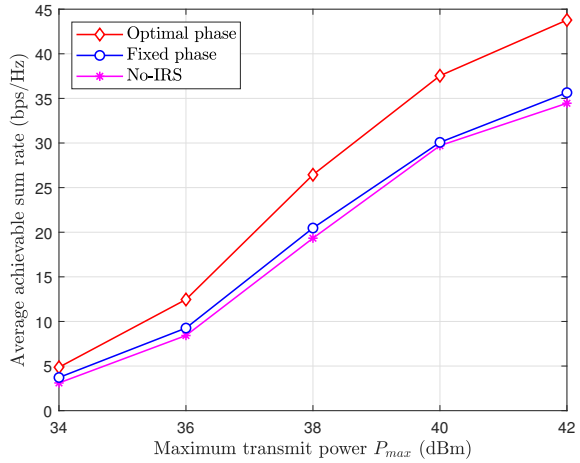

(a)

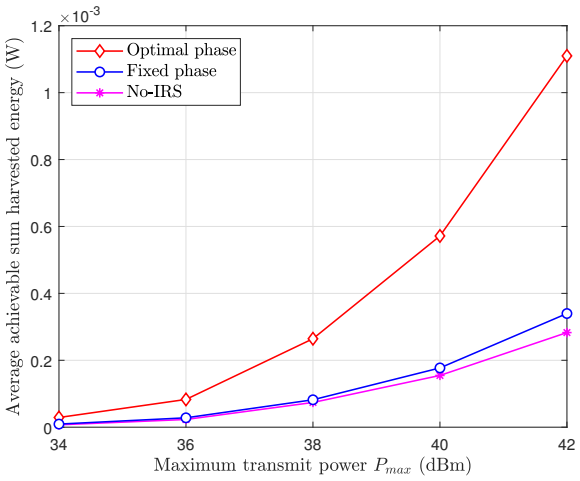

(b)

Figure 4. Average achievable SR and average SHE of users versus the maximum TP of the BS.

Example 3: By applying Algorithm 3 to solve the MOOP, we investigate the tradeoffs between the achievable SR and the SHE of the users. Figure 5 provides the numerical results of the average achievable SR and SHE with various maximum TP $P_{max} = \{38, 40, 42\}$ dBm, which are obtained by changing the quantities of weighted parameters $\omega_1 \in \{0.1, 0.3, 0.5, 0.7, 0.9\}$, $\omega_2 = 1 - \omega_1$, and $\tau = 0.005$. The results depicted in Figure 5 indicate that the achievable SR reduces as the achievable SHE increases. This proves that the SRM and the SHEM problems do not coincide. Specifically, the results in Figure 5 show that for the region of the low SHE, a small increase in the achievable SHE results in the small decline in the achievable SR. In contrast, when the achievable SHE reaches a certain level, a small increase in the achievable SHE leads to

the significant decrease in the achieve SR. Therefore, the numerical results in Figure 5 demonstrate the insightful tradeoff between the achievable SR and the achievable SHE, which allows communication system designers to control the system performance by setting the appropriate weighted parameters to meet the specific requirements. The results also show that the Pareto region is enlarged as the maximum TP P_{max} increases. In other words, both achievable SR and SHE are improved as P_{max} increases.

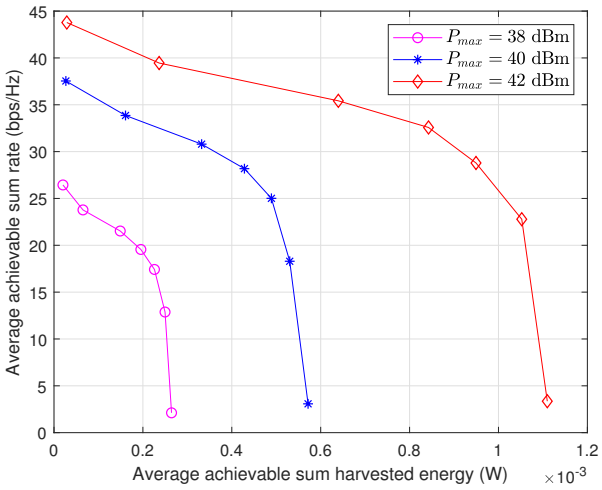

Figure 5. Performance tradeoffs between average achievable SR and SHE obtained by the MOOP algorithm.

6 Conclusions

In this paper, we have explored the tradeoffs between the achievable SR and SHE of the users in an IRS-assisted MU-MIMO SWIPT system under the maximum TP budget constraint, the minimum data rate, and HE requirements at each user by optimizing the BS TPMs, the user PSRs, and the IRS PSM. To obtain the insightful tradeoff between the achievable SR and SHE, we have formulated the design problem as a MOOP, then applied the MWT approach to cast the MOOP into a SOOP. Considering the practical NLEH model, the resulting optimization problems are challenging to solve due to their non-linearity and non-convexity w.r.t. the coupled design variables. To render the OPs amenable, we have applied the AO method to partition the original OPs into the sub-problems. Then, we have derived effective surrogate functions to recast the sub-problems into convex OPs. The numerical simulation results have illustrated the efficient convergence of the proposed AO algorithm for the SOOPs and MOOP. They have also demonstrated that the systems using the IRS with optimal PSM can provide significant benefits in SR and SHE performance gains compared to the counterparts without using the IRS or with a deployment of the IRS with fixed PSM. Moreover, the numerical results have revealed the insightful tradeoffs between the achievable SR and SHE in the considered system.

Acknowledgements

This research is funded by Vietnam National Foundation for Science and Technology Development (NAFOSTED) under grant number 102.04-2021.17.

References

[1] F. A. Pereira de Figueiredo, "An overview of massive MIMO for 5G and 6G," *IEEE Latin America Transactions*, vol. 20, no. 6, pp. 931–940, 2022.

[2] S. Gong, X. Lu, D. T. Hoang, D. Niyato, L. Shu, D. I. Kim, and Y.-C. Liang, "Toward Smart Wireless Communications via Intelligent Reflecting Surfaces: A Contemporary Survey," *IEEE Communications Surveys & Tutorials*, vol. 22, no. 4, pp. 2283–2314, Jun. 2020.

[3] Q. Wu and R. Zhang, "Towards Smart and Reconfigurable Environment: Intelligent Reflecting Surface Aided Wireless Network," *IEEE Communications Magazine*, vol. 58, no. 1, pp. 106–112, Jan. 2020.

[4] M. Di Renzo, A. Zappone, M. Debbah, M.-S. Alouini, C. Yuen, J. de Rosny, and S. Tretyakov, "Smart Radio Environments Empowered by Reconfigurable Intelligent Surfaces: How It Works, State of Research, and The Road Ahead," *IEEE Journal on Selected Areas in Communications*, vol. 38, no. 11, pp. 2450–2525, Jul. 2020.

[5] C. Pan, H. Ren, K. Wang, M. Elkashlan, A. Nallanathan, J. Wang, and L. Hanzo, "Intelligent Reflecting Surface Aided MIMO Broadcasting for Simultaneous Wireless Information and Power Transfer," *IEEE Journal on Selected Areas in Communications*, vol. 38, no. 8, pp. 1719–1734, Aug. 2020.

[6] W. Yan, X. Yuan, and X. Kuai, "Passive Beamforming and Information Transfer via Large Intelligent Surface," *IEEE Wireless Communications Letters*, vol. 9, no. 4, pp. 533–537, Dec. 2020.

[7] X. Yu, D. Xu, D. W. K. Ng, and R. Schober, "Power-Efficient Resource Allocation for Multiuser MISO Systems via Intelligent Reflecting Surfaces," in *Proceedings of the 2020 IEEE Global Communications Conference*, Dec. 2020, pp. 1–6.

[8] H. Niu, Z. Chu, F. Zhou, Z. Zhu, L. Zhen, and K.-K. Wong, "Robust Design for Intelligent Reflecting Surface Assisted Secrecy SWIPT Network," *IEEE Transactions on Wireless Communications*, pp. 4133 – 4149, Nov. 2021.

[9] Z. Yang and Y. Zhang, "Optimal SWIPT in RIS-Aided MIMO Networks," *IEEE Access*, vol. 9, pp. 112 552–112 560, Jul. 2021.

[10] N. Garg, A. Rudraksh, G. Sharma, and T. Ratnarajah, "Improved rate-energy trade-off for SWIPT using chordal distance decomposition in interference alignment networks," *IEEE Transactions on Green Communications and Networking*, pp. 917 – 929, Sep. 2021.

[11] X. Zhou, R. Zhang, and C. K. Ho, "Wireless information and power transfer: Architecture design and rate-energy tradeoff," *IEEE Transactions on Communications*, vol. 61, no. 11, pp. 4754–4767, Oct. 2013.

[12] R. Zhang and C. K. Ho, "MIMO broadcasting for simultaneous wireless information and power transfer," *IEEE Transactions on Wireless Communications*, vol. 12, no. 5, pp. 1989–2001, Mar. 2013.

[13] Q. Wu and R. Zhang, "Joint active and passive beamforming optimization for intelligent reflecting surface assisted SWIPT under QoS constraints," *IEEE Journal on Selected Areas in Communications*, vol. 38, no. 8, pp. 1735–1748, Jul. 2020.

[14] S. Zargari, A. Khalili, Q. Wu, M. Robat Mili, and D. W. K. Ng, "Max-min fair energy-efficient beamforming design for intelligent reflecting surface-aided SWIPT systems with non-linear energy harvesting model," *IEEE Transac-*

tions on Vehicular Technology, vol. 70, no. 6, pp. 5848–5864, June 2021.
[15] P. V. Quyet and H. H. Kha, "Energy harvesting maximization for multiuser MIMO SWIPT systems with intelligent reflecting surfaces," *Telecommunication Systems*, vol. 80, no. 4, p. 497–511, 2022.
[16] A. Zappone, M. Di Renzo, X. Xi, and M. Debbah, "On the optimal number of reflecting elements for reconfigurable intelligent surfaces," *IEEE Wireless Communications Letters*, vol. 10, no. 3, pp. 464–468, Oct. 2021.
[17] M. Zhang, L. Tan, K. Huang, and L. You, "On the tradeoff between energy efficiency and spectral efficiency in RIS-aided multi-user MISO downlink," *Electronics*, vol. 10, no. 11, May 2021.
[18] A. Khalili, S. Zargari, Q. Wu, D. W. K. Ng, and R. Zhang, "Multi-objective resource allocation for IRS-aided SWIPT," *IEEE Wireless Communications Letters*, vol. 10, no. 6, pp. 1324–1328, June 2021.
[19] E. Bjornson, E. A. Jorswieck, M. Debbah, and B. Ottersten, "Multiobjective signal processing optimization: The way to balance conflicting metrics in 5G systems," *IEEE Signal Processing Magazine*, vol. 31, no. 6, pp. 14–23, Nov. 2014.
[20] W.-Y. Chen, B.-S. Chen, and W.-T. Chen, "Multiobjective beamforming power control for robust SINR target tracking and power efficiency in multicell MU-MIMO wireless system," *IEEE Transactions on Vehicular Technology*, vol. 69, no. 6, pp. 6200–6214, 2020.
[21] R. T. Marler and J. S. Arora, "Survey of multi-objective optimization methods for engineering," *Structural and Multidisciplinary Optimization*, vol. 26, no. 6, pp. 369–395, Mar. 2004.
[22] L. Wei, C. Huang, G. C. Alexandropoulos, C. Yuen, Z. Zhang, and M. Debbah, "Channel estimation for RIS-empowered multi-user MISO wireless communications," *IEEE Transactions on Communications*, vol. 69, no. 6, pp. 4144–4157, 2021.
[23] B. Zheng, C. You, W. Mei, and R. Zhang, "A survey on channel estimation and practical passive beamforming design for intelligent reflecting surface aided wireless communications," *IEEE Communications Surveys & Tutorials*, vol. 24, no. 2, pp. 1035–1071, 2022.
[24] B. Clerckx, R. Zhang, R. Schober, D. W. K. Ng, D. I. Kim, and H. V. Poor, "Fundamentals of wireless information and power transfer: From RF energy harvester models to signal and system designs," *IEEE Journal on Selected Areas in Communications*, vol. 37, no. 1, pp. 4–33, Jan. 2019.
[25] E. Boshkovska, D. W. K. Ng, N. Zlatanov, and R. Schober, "Practical non-linear energy harvesting model and resource allocation for SWIPT systems," *IEEE Communications Letters*, vol. 19, no. 12, pp. 2082–2085, Dec. 2015.
[26] E. Boshkovska, D. W. K. Ng, N. Zlatanov, A. Koelpin, and R. Schober, "Robust resource allocation for MIMO wireless powered communication networks based on a non-linear EH model," *IEEE Transactions on Communications*, vol. 65, no. 5, pp. 1984–1999, May 2017.
[27] H. H. M. Tam, H. D. Tuan, A. A. Nasir, T. Q. Duong, and H. V. Poor, "MIMO energy harvesting in full-duplex multi-user networks," *IEEE Transactions on Wireless Communications*, vol. 16, no. 5, pp. 3282–3297, Mar. 2017.
[28] M. Grant, S. Boyd, and Y. Ye, "CVX: Matlab software for disciplined convex programming," 2008.
[29] X. D. Zhang, *Matrix analysis and applications*. Cambridge University Press, 2017.
[30] L. Zhang, Y. Wang, W. Tao, Z. Jia, T. Song, and C. Pan, "Intelligent reflecting surface aided MIMO cognitive radio systems," *IEEE Transactions on Vehicular Technology*, vol. 69, no. 10, pp. 11 445–11 457, Oct. 2020.
[31] L. Dong, H.-M. Wang, and H. Xiao, "Secure cognitive radio communication via intelligent reflecting surface," *IEEE Transactions on Communications*, vol. 69, no. 7, pp. 4678–4690, Apr. 2021.
[32] Y. Ge and J. Fan, "Robust secure beamforming for intelligent reflecting surface assisted full-duplex MISO systems," *IEEE Transactions on Information Forensics and Security*, vol. 17, pp. 253–264, Dec. 2022.
[33] J. Song, P. Babu, and D. P. Palomar, "Optimization methods for designing sequences with low autocorrelation sidelobes," *IEEE Transactions on Signal Processing*, vol. 63, no. 15, pp. 3998–4009, Apr. 2015.
[34] T.-V. Nguyen, V.-D. Nguyen, D. B. da Costa, and B. An, "Hybrid user pairing for spectral and energy efficiencies in multiuser MISO-NOMA networks with SWIPT," *IEEE Transactions on Communications*, vol. 68, no. 8, pp. 4874–4890, Aug. 2020.
[35] V.-D. Nguyen, H. D. Tuan, T. Q. Duong, H. V. Poor, and O.-S. Shin, "Precoder design for signal superposition in MIMO-NOMA multicell networks," *IEEE Journal on Selected Areas in Communications*, vol. 35, no. 12, pp. 2681–2695, Dec. 2017.
[36] B. Lyu, P. Ramezani, D. T. Hoang, S. Gong, Z. Yang, and A. Jamalipour, "Optimized energy and information relaying in self-sustainable IRS-empowered WPCN," *IEEE Transactions on Communications*, vol. 69, no. 1, pp. 619–633, Jan. 2021.

Pham Van Quyet received the B.S. degree from Telecommunications University, Vietnam, in 2009, and the M.Eng. degree from the Posts and Telecommunications Institute of Technology, Vietnam, in 2014, all in Telecommunications Engineering. He is currently pursuing the Ph.D. degree in Telecommunications Engineering at Ho Chi Minh City University of Technology, Vietnam. His current research interests include intelligent reflecting surface (IRS), energy harvesting, signal processing and wireless communication systems.

Ha Hoang Kha received the B.Eng. and M.Eng. degrees from Ho Chi Minh City University of Technology, in 2000 and 2003, respectively, and the Ph.D. degree from the University of New South Wales, Sydney, Australia, in 2009, all in Electrical Engineering and Telecommunications. From 2000 to 2004, he was a research and teaching assistant with the Department of Electrical and Electronics Engineering, Ho Chi Minh City University of Technology. He was a visiting research fellow at the School of Electrical Engineering and Telecommunications, the University of New South Wales, Australia, from 2009 to 2011. He was a postdoctoral research fellow at the Faculty of Engineering and Information Technology, University of Technology Sydney, Australia from 2011 to 2013. He is currently a lecturer at the Faculty of Electrical and Electronics Engineering, Ho Chi Minh City University of Technology, VNU-HCM, Vietnam. His research interests are in digital signal processing and wireless communications, with a recent emphasis on convex optimization and machine learning techniques in signal processing for wireless communications.